Acta Oceanol. Sin., 2021, Vol. 40, No. 3, P. 34–45
https://doi.org/10.1007/s13131-021-1710-9
http://www.hyxb.org.cn
E-mail: hyxbe@263.net

Observational characteristics and dynamic mechanism of low-salinity water lens for the offshore detachment of the Changjiang River diluted water in August 2006

Zhenyu Liu[1], Wenjing Zhang[1]*, Xuejun Xiong[2], Shouxian Zhu[3]

[1] College of Meteorology and Oceanography, National University of Defense Technology, Nanjing 211101, China

[2] First Institute of Oceanography, Ministry of Natural Resources, Qingdao 266061, China

[3] College of Oceanography, Hohai University, Nanjing 211101, China

Received 13 April 2020; accepted 22 June 2020

Abstract

The Changjiang River diluted water (CDW) spreads into the East China Sea (ECS) primarily in a plume pattern, although in some years, low-salinity water lenses (LSWLs) detach from the main body of the CDW. *In-situ* observations indicate that in August 2006, a LSWL detached from the main body of the CDW near the river mouth. In this paper, the effects of winds, tides, baroclinity and upwelling on LSWLs are explored with a three-dimensional model. The results show that: (1) winds play a crucial role in these detachment events because wind-induced northerly Eulerian residual currents impose an uneven force on the CDW and cut it off, thus forming a LSWL; (2) upwelling carries high-salinity water from the lower layer to the upper layer, truncating the low-salinity water tongue vertically, which is conducive to the detachment and maintenance of LSWLs; and (3) upwelling during the evolution of a LSWL is caused by the combined effects of winds and tides. The influences of wind-induced upwelling are mainly near the shore, whereas the upwelling along the 30 m isobath is predominantly affected by tides, with the effect increasing from neap tide to spring tide.

Key words: Changjiang River diluted water, low-salinity water lens, numerical simulation, observational characteristics, dynamic mechanism, upwelling

Citation: Liu Zhenyu, Zhang Wenjing, Xiong Xuejun, Zhu Shouxian. 2021. Observational characteristics and dynamic mechanism of low-salinity water lens for the offshore detachment of the Changjiang River diluted water in August 2006. Acta Oceanologica Sinica, 40(3): 34–45, doi: 10.1007/s13131-021-1710-9

1 Introduction

The Changjiang River (also known as the Yangtze River) diluted water (CDW) has a significant impact on the circulation structure, water mass composition, and sediment deposition in the Yellow Sea (YS) and the East China Sea (ECS). The CDW generally enters the YS and ECS and spreads out in a plume and the surface salinity around the Changjiang River Estuary shows significant seasonal variation (Wu et al., 2020) although observations indicate that isolated low-salinity water lenses (LSWLs) occasionally detach from the main body of the CDW (Pu, 2002). These LSWLs are an important factor causing area eutrophication and hypoxia in the Changjiang River Estuary and its adjacent waters (Xuan et al., 2012); thus, this topic has attracted considerable attention from ecological dynamics scientists (Kim et al., 2009; Li et al., 2002, 2019; Zhang et al., 2019). Studies on the LSWL mechanism have been conducted. By analyzing observed data from the area east of Cheju Island, Lie et al. (2003) suggested that the separation of CDW patches from the shallow shelf area and upwelling favorable southerly winds in summer are the main contributors. Chen et al. (2008) used the unstructured-grid, Finite-Volume Coastal Ocean Model (FVCOM) to simulate a LSWL in the sea west of 123°E and proposed that the detachment of this LSWL is associated with eddies generated by baroclinic instability across the plume front. Using the Regional Ocean Modeling System (ROMS), Moon et al. (2010) simulated a LSWL under ideal wind, tide and runoff conditions and suggested that the strengthening of tidal mixing during the spring tide plays an important role in the detachment of the LSWL. Wu et al. (2011) indicated that strong upwelling during the spring tide can disconnect part of the Changjiang River plume. Xuan et al. (2012) used the MIT general circulation model (MITgcm) to analyze the dynamic mechanism responsible for LSWL detachment and indicated that wind mixing, wind-driven northward currents and wind-induced upwelling are the three driving forces underlying the detachment of the LSWL. Using the POM-σ-z model, Zhang et al. (2014a, b) demonstrated that southerly winds push the CDW northeastward and cut it off, thereby detaching the LSWL, and they also showed that the intensified tidal mixing during the spring tide plays a major role in the LSWL detachment process. Peng et al. (2014) indicated that LSWL detachment depends on different combinations of wind and tide conditions and that southerly winds during the spring tide are the main contributors to LSWL detachment.

Both winds and tides are generally believed to have important influences on LSWL detachment. In recent years, upwelling water has been found in the detachment region (Moon et al., 2010; Wu et al., 2011; Xuan et al., 2012). Although the magnitude of the upwelling velocity is small, an upwelling can carry saline

Foundation item: The National Natural Science Foundation of China under contract No. 41376012.
*Corresponding author, E-mail: zhangwj-lgd@sohu.com

seawater from the bottom to the surface and therefore can significantly impact the distribution of salinity, which may be conducive to detachment. However, the role of upwelling water on detaching the LSWL has not been thoroughly explored; thus, the effects and dynamic mechanism of upwelling during the evolution of the LSWL need to be further studied. In this paper, the dynamic mechanism of the LSWL observed in August 2006 is studied with a focus on the effects of upwelling on the LSWL.

2 Characteristic analysis of the LSWL in 2006

The observed data were obtained from a cruise survey carried out during July 27 to August 12, 2006. During the cruise, conductivity-temperature-depth (CTD) instruments were used in the field program to measure the vertical profiles of water temperature and salinity. The path of the cruise extended alongshore from 29.8°N to 32.3°N and offshore from 121°E to 128°E. The sea near the Changjiang River Estuary was the key observation area, and the minimum latitudinal resolution was (1/9)°.

The distribution of surface salinity in the survey area is shown in Fig. 1a. The salinity front (less than 22) near the Changjiang River Estuary extends toward the southeast, thus reflecting the jet pattern of the CDW (Wang et al., 2012), whereas the CDW from the Changjiang River Estuary extends northeastward in a plume pattern. The detachment of the LSWL occurs on the interior side of the river plume at approximately 31.8°N, 122.7°E. The LSWL isolated by the 22 isohaline has an elliptical shape, and the value of the central closed isohaline is 20. The size of the LSWL (the diameter of the long axis of the outermost closed isohaline) is 70 km. Figure 1b shows the vertical salinity distribution along Line A through the center of the LSWL. The upper salinity stratification structure is obvious, and the lower water is mixed uniformly. Additionally, the 32 isohaline obviously descends from west to east. This phenomenon was discussed by Zhao (1993) in consideration of upwelling.

The distribution of surface temperature is depicted in Fig. 2a. There is a clear, cold water belt between 122°E and 123°E that has two cold centers. The first cold center is located at the junction of the Changjiang River Estuary and Hangzhou Bay, while the second cold center is located northeast of the Changjiang River Estuary on the west side of the LSWL. Low surface temperature reveals the spread of cold water and thus the range of upwelling (Li et al., 2018). Figure 2b shows the vertical temperature distribution along Line A, and it consists of an upper mixed layer, a thermocline layer, and a lower mixed layer. The thicknesses of the upper mixed layer and the thermocline layer are both 5–10 m, and the isotherm below the thermocline gradually rises from east to west. Similar to the 32 isohaline, the 25°C isotherm rises from east to west. Both the isotherms and the isohalines suggest that cold and saline deep water upwells along the bottom slope.

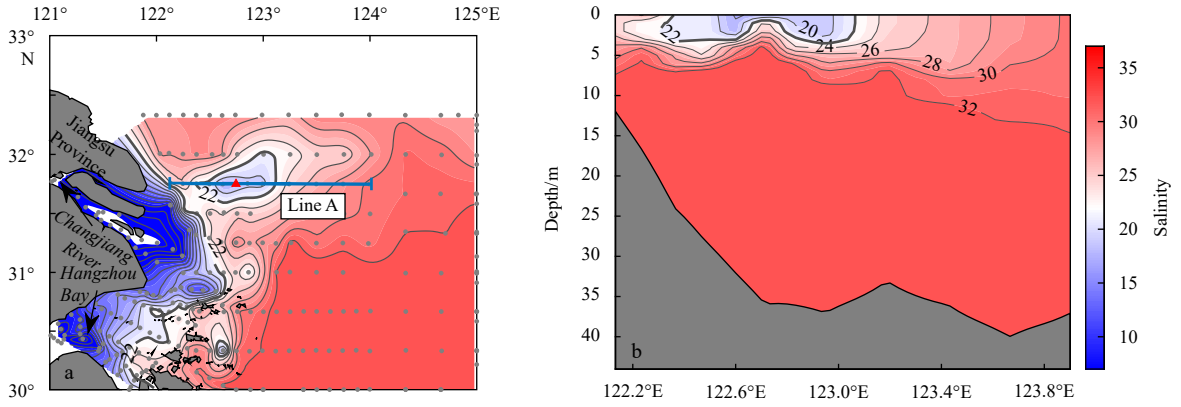

Fig. 1. Surface salinity distribution observed in the summer of 2006 with gray circles showing the observation sites (a) , and vertical salinity distribution along Line A (b). The red triangle in a indicates the center of the LSWL; and the thick solid line in b is the 22 isohaline.

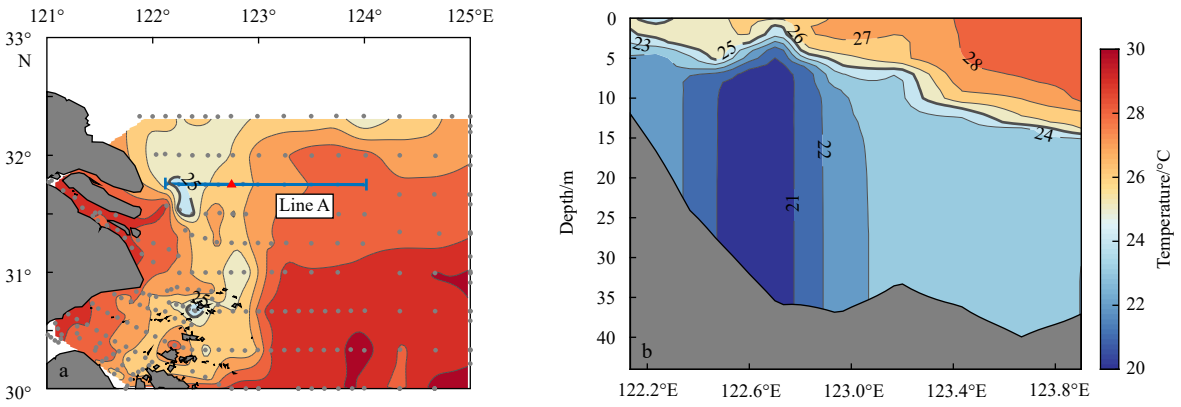

Fig. 2. Surface temperature distribution observed in the summer of 2006 with gray circles showing the observation sites (a), and vertical temperature distribution along Line A (b). The red triangle in a indicates the center of the LSWL, and the thick solid line in b is the 25°C isotherm.

3 Numerical simulation of the LSWL in 2006

The POM-σ-z model (Zhang et al., 2011), which is developed from the Princeton Ocean Model (Blumberg and Mellor, 1987), is used in the LSWL simulation. As shown in Fig. 3a, the σ coordinate is employed for the current calculation, and the transform is

$$\sigma_1 = \frac{z-\eta}{H+\eta} = \frac{z-\eta}{D}, \tag{1}$$

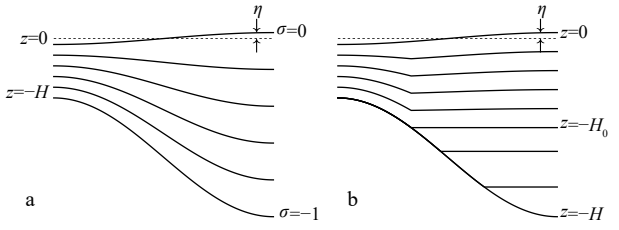

Fig. 3. σ coordinate for the current calculation (a), and σ-z coordinate for the salinity calculation (b).

where H is the bottom topography, η is the surface elevation, and $D=H+\eta$ is the total water depth. As shown in Fig. 3b, the σ-z coordinate is used for the salinity calculation. The seawater is vertically divided into two parts, where $z=-H_0$ is the interface. The σ coordinate is used in the water above the interface, and the corresponding transform is expressed as

$$\begin{cases} \sigma_2 = \dfrac{z-\eta}{H+\eta} = \dfrac{z-\eta}{D_1} & H \leqslant H_0 \\ \sigma_2 = \dfrac{z-\eta}{H_0+\eta} = \dfrac{z-\eta}{D_1} & H > H_0 \end{cases}. \tag{2}$$

In contrast, the z coordinate is used in the water below the interface.

The Eulerian-Lagrangian method (ELM) is used to address the effect of the current on salinity. The salinity equation used in the ELM in σ-z coordinates is

$$\frac{\mathrm{d}S}{\mathrm{d}t} = F, \tag{3}$$

where $\dfrac{\mathrm{d}S}{\mathrm{d}t}$ is the total derivative of salinity, which describes the change in salinity over time. F is the turbulent mixing term. The expression of F is

$$\begin{cases} F = \dfrac{1}{D_1^2}\dfrac{\partial}{\partial\sigma}\left(K_H\dfrac{\partial S}{\partial\sigma}\right) + F_S & z \geqslant -H_0 \\ F = \dfrac{\partial}{\partial z}\left(K_H\dfrac{\partial S}{\partial z}\right) + F_S & z < -H_0 \end{cases}, \tag{4}$$

where F_S is the horizontal turbulent mixing term. If a water particle goes from point P at time $n\Delta t$ to point Q at time $(n+1)\Delta t$, then we have the expression as

$$S^{n+1}(Q) = S^n(P) + F\Delta t. \tag{5}$$

The change of salinity at point Q at time $(n+1)\Delta t$ is caused by two kinds of dynamics. One is convection. The water particle at point Q at time $(n+1)\Delta t$ is substituted by one at point P at time $n\Delta t$; therefore, the salinity at point Q at time $(n+1)\Delta t$ keeps the character at point P at time $n\Delta t$. The other is eddy diffusion. To determine the effect of current on the salinity calculation, the location of point P must be determined.

The method of determining the location of point P is as follows:

$$\begin{cases} x(P) = x(Q) - u^{n+1}(Q)\Delta t \\ y(P) = y(Q) - v^{n+1}(Q)\Delta t \\ \sigma(P) = \sigma(Q) - \omega^{n+1}(Q)\Delta t \end{cases}, \tag{6}$$

where $u^{n+1}(Q)$, $v^{n+1}(Q)$, and $\omega^{n+1}(Q)$ are from the linear interpolation of the current at time $(n+1)\Delta t$. $S^n(P)$ is calculated from the interpolation of salinity at time $n\Delta t$. Zhu et al. (2001) advanced this method by combining first-order and second-order Lagrange interpolations, and this advanced approach is used in this paper.

The computational domain covers the Bohai Sea, the YS and the ECS (Fig. 4a). The numerical grids are shown in Fig. 4b. The minimum and maximum distances between the grids are 1 540 m and 25 000 m, respectively. In the vertical direction, the current calculation uses 20 vertical σ layers. The salinity calculation takes place in the σ-z layer, which has 8 uniform σ layers in the upper waters and 24 z layers in the lower waters. The interface between these two parts is at a depth of 25 m.

For convenience, the numerical simulation of the LSWL in summer 2006 is called CASE06, which couples the tidal currents and circulation in consideration of runoff, winds, tides (the M_2, S_2, K_1 and O_1 tidal constituents), the Taiwan Warm Current (TWC), the Kuroshio, the Tsushima Warm Current, and the baroclinic effect. The Changjiang River discharge is obtained from the monthly averaged flux at the Datong hydrometric station, which is ~640 km upstream from the river mouth. The wind force is obtained from 6-hourly NCEP/NCAR reanalyzed wind data. The climatological averages of the salinity and sea temperature in summer are used as the original field data, and the sea temperature does not change with time in the calculation. The calculation coupled the tidal current and the circulation begins on July 2, 2006, and runs simultaneous with the salinity calculation on July 9, 2006. The numerical scheme of CASE06 is similar to that of a previous study (Zhang et al., 2011), which introduced more details of the model and its validation.

Figure 5 shows part of the simulated surface salinity. Beginning on August 3, low-salinity water (less than 30) extended northeastward from the Changjiang River mouth in a tongue shape. At 2:00 on August 7, the LSWL detached from the interior side of the river plume at approximately 32°N, 122.9°E and then gradually moved northeastward. After August 10, the central position of the LSWL was nearly fixed. Finally, the LSWL disappeared at 15:00 on August 19. During August 7 to 19, the value of the central closed isohaline increased from 18 to 28 and the size of the LSWL was generally 20–85 km. The LSWL disappeared briefly several times but consistently maintained a tongue shape.

Compared with the observed characteristics, the real-case simulation of the detachment of the LSWL in August 2006 shows that the shape of the LSWL remained basically the same. Numerical experiments to further reveal the mechanism of detachment are therefore justifiable.

4 Analysis of the LSWL dynamic mechanism

In this section, seven experiments (Table 1) are designed to examine the influences of winds, tides, vertical mixing, and up-

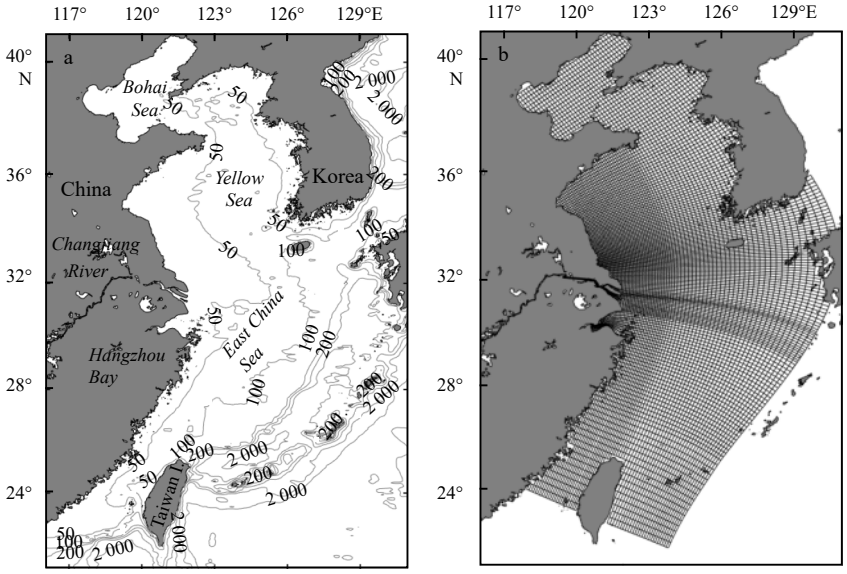

Fig. 4. Map of the East China Sea, the Yellow Sea and the Bohai Sea (a), and model domain and horizontal curvilinear coordinate system (b). Bathymetry contours are given in unit of m.

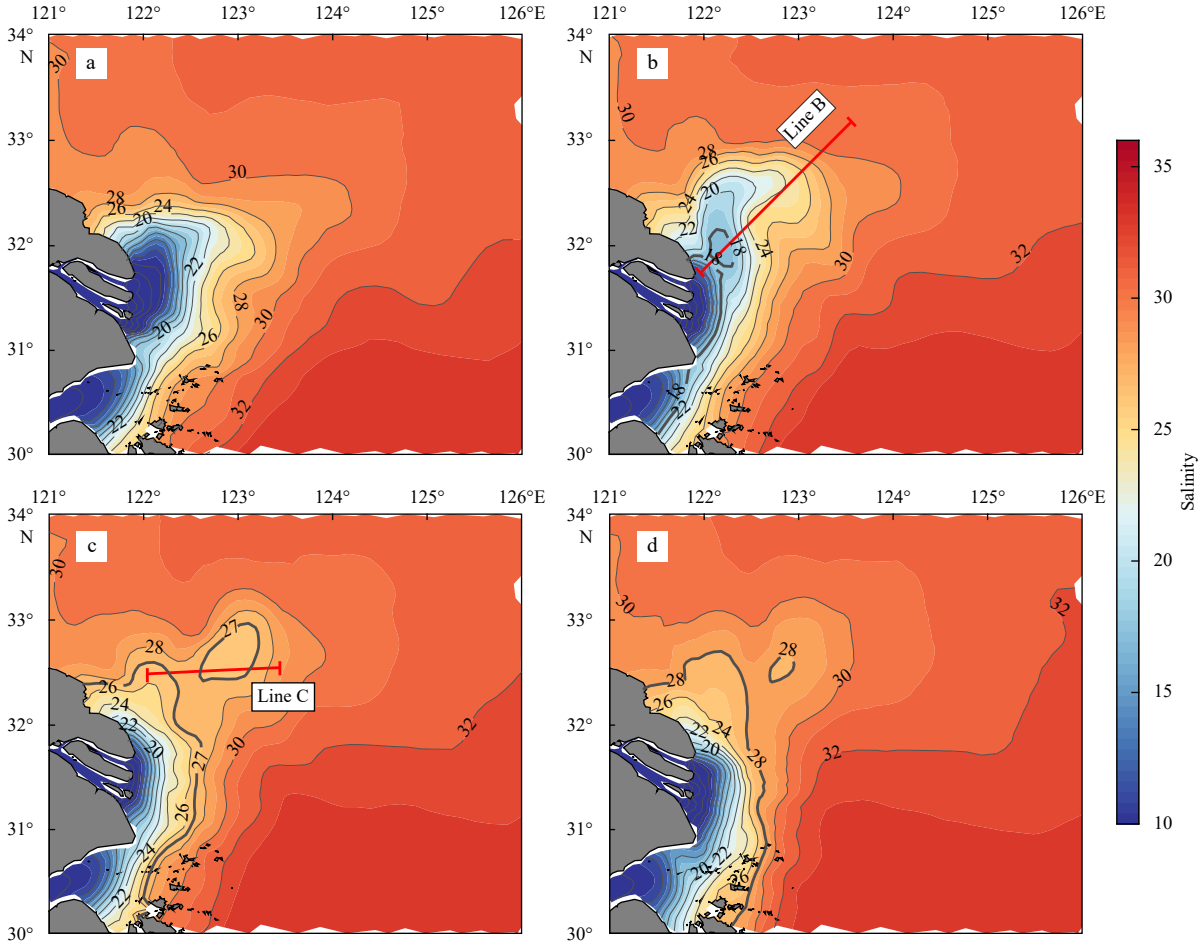

Fig. 5. Surface distribution of salinity in CASE06 at 03:00 on August 3 (a) , 02:00 on August 7 (b), 01:00 on August 12 (c) and 00:00 on August 19 (d).

welling and the baroclinic effect on the LSWL. We take CASE06 as the control test. Based on CASE06, the arrangement of CASE06a removes the wind forcing to eliminate its influence. CASE06b uses the same model settings as CASE06, although the wind is changed to a steady southerly wind of 4 m/s. For CASE06c and CASE06d, the effects of tides and vertical mixing are removed, re-

Table 1. Summary of the numerical experiments conducted to analyze the LSWL detachment mechanism[1)]

Case	Wind	Tide	Vertical mixing	Vertical velocity	Baroclinity
CASE06	Y	Y	Y	Y	Y
CASE06a	N	Y	Y	Y	Y
CASE06b	Y[2)]	Y	Y	Y	Y
CASE06c	Y	N	Y	Y	Y
CASE06d	Y	Y	N	Y	Y
CASE06e	Y	Y	Y	N	Y
CASE06f	Y	Y	Y	Y	N
CASE06g	Y	Y	Y	Y	Y[3)]

Note: [1)] Y means that the dynamic factors are considered in the simulation, and N means that dynamic factors are excluded from the simulation. [2)] The wind is changed to a steady southerly wind of 4 m/s. [3)] The BPG is calculated by the climatological average of the salinity and sea temperature.

spectively, while all other physical processes remain intact. The vertical velocity in the z coordinate (w_z) of CASE06e is set to 0 (the setting method is explained in detail in Section 4.3). For CASE06f, the only modification to the model configuration is setting the baroclinic pressure gradient (BPG) term to 0; and for CASE06g, the BPG term is calculated by the climatological average for the salinity and sea temperature. In addition, we also verified the roles of the Changjiang River discharge and TWC in the occurrence of detachment (not shown). To discuss the effects of runoff and the TWC, experiments were conducted in which both the Changjiang River discharge and the TWC are both doubled and halved. The results (not shown) show that Changjiang River discharge and TWC have little effect on detachment; therefore, these experiments are not included in Table 1.

4.1 *Winds and the detachment mechanism*

Figure 6 shows the NCEP 5-day average wind from August 2 to 21, 2006. Given that LSWL detachments occur within the 0–10 m layer and wind plays an important role in currents, the vertical average of the currents in the 0–10 m layer is used to analyze the current during the detachment process (Xuan et al., 2012). Based on the simulated results of CASE06, the Eulerian residual current (ERC) is calculated. Figure 7 shows the 5-day average ERC in the 0–10 m layer. During August 2 to 6, the CDW expansion area was controlled by a southeasterly wind with a mean speed of 4.0–5.5 m/s (Fig. 6a). The ERC between 31°N and 33°N had an average speed of 10 cm/s and was divided into two parts by the 30 m isobath: a western part, in which the ERC was oriented mainly toward the north, and an eastern part, in which the ERC was oriented mainly

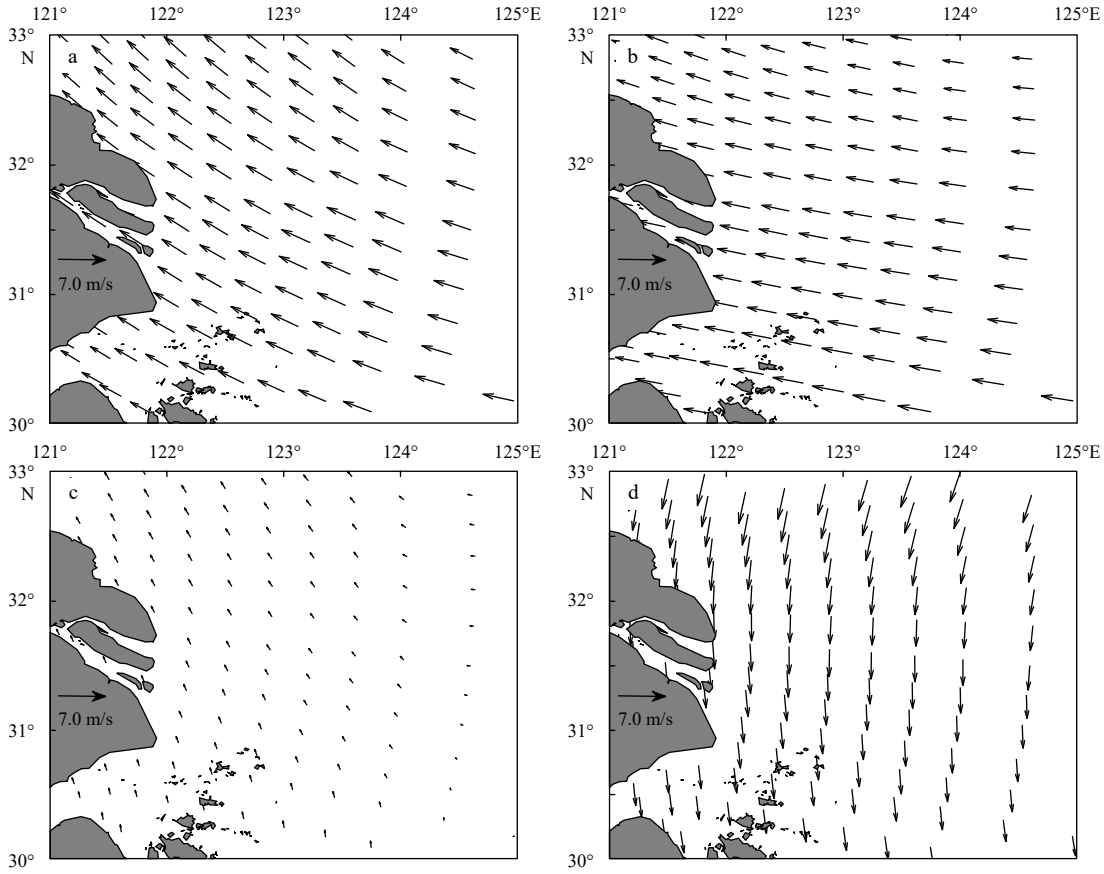

Fig. 6. Average wind vectors during August 2 to 6 (a), August 7 to 11 (b), August 12 to 16 (c) and August 17 to 21 (d).

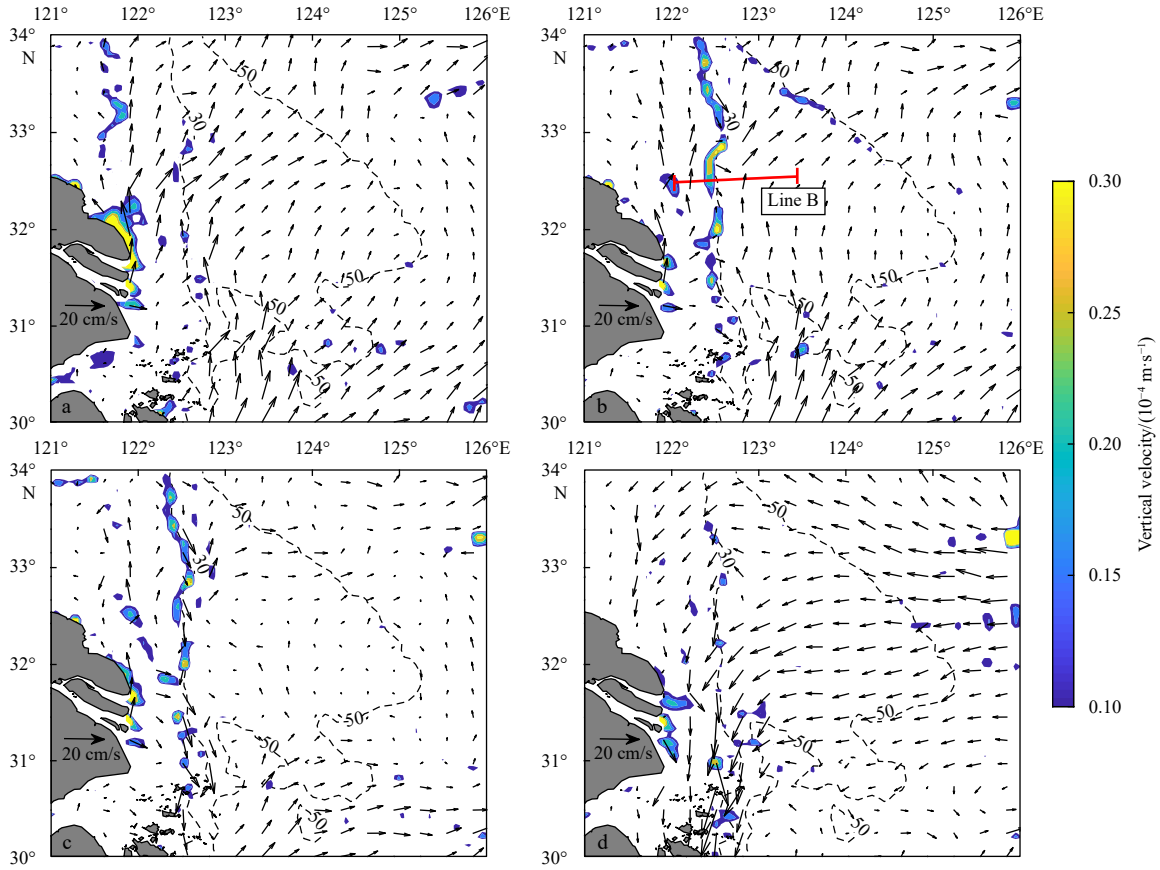

Fig. 7. Distributions of the 5-day average velocity in the 0–10 m layer during August 2 to 6 (a), August 7 to 11 (b), August 12 to 16 (c) and August 17 to 21 (d). Dashed lines are the 30 m and 50 m isobaths. Filled contours indicate the distribution of the vertical velocity. The vectors represent the Eulerian residual current.

toward the northeast (Fig. 7a). During August 7 to 11, the sea surface was controlled by a southeasterly wind with a mean speed of 3.5–6.0 m/s (Fig. 6b). The horizontal current structure was similar to that during the last phase (August 2 to 6), although the velocity was slightly weakened (Fig. 7b). During August 12 to 16, the southeasterly wind weakened and its average speed was less than 1 m/s (Fig. 6c), which weakened the ERC significantly (Fig. 7c). During August 17 to 21, a northerly wind prevailed with an average speed of 4.0–6.0 m/s (Fig. 6d). The ERC flow mainly toward the southwest at a speed of approximately 13 cm/s (Fig. 7d).

The evolutionary characteristics of the wind, ERC and LSWL revealed a close relationship. During August 2 to 11, forced by the sustained southeasterly wind, the ERC vectors showed differences on both sides of the 30 m isobath, with a northward current on the left side and a current mainly to the northeast on the right side. The nonuniform ERC imposed an uneven northward force on the CDW and cut it off, which facilitated LSWL detachment (Xuan et al., 2012; Zhang et al., 2014b). During August 12 to 16, the light southeasterly wind weakened the ERC, which stabilized the LSWL. During August 17 to 21, the strong northerly wind caused the ERC to flow southward; and under the effect of this current, the CDW receded to the south, which caused the LSWL to disappear.

Two numerical simulations, CASE06a and CASE06b, were conducted to test the effects of winds on the LSWL. The easterly and northeasterly offshore expansions of the CDW in CASE06a were weaker than those in CASE06 and there was no LSWL (not shown). However, two detachment events appeared in CASE06b: the first detachment occurred on the interior side of the river plume and lasted from 05:00 on August 7 to 14:00 on August 9 (Fig. 8), while the second detachment occurred at the same location as the first detachment but lasted from 03:00 on August 22 to 03:00 on August 23.

These two numerical simulations considered either no wind

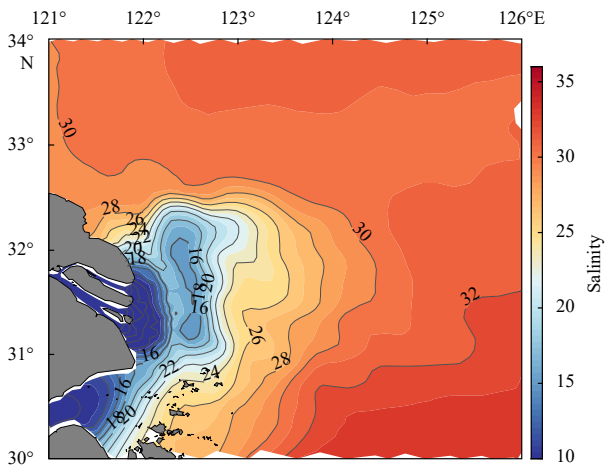

Fig. 8. Simulated surface salinity at 05:00 on August 7 in CASE06b.

or only a light southerly wind. In comparison with CASE06, the simulation results showed either no detachment or a detachment region relatively close to the Changjiang River Estuary. These results indicated that the southerly wind had an important impact on the detachment and offshore movement of the LSWL.

4.2 *Tides and the detachment mechanism*

The tidal data in this section are taken from the tide table produced by the United Kingdom (UK) Hydrographic Office. Figure 9 shows the tide level at Lühuashan station (30.82°N, 122.6°E) in August 2006. Neap tides occurred on August 3 and 18, whereas spring tides occurred on August 10 and 25. The LSWL detached on August 7, which was the time of the transition from neap tide to spring tide.

To verify the role of tides in detachment, CASE06c was conducted. The results show that no LSWL was detached in CASE06c (not shown), confirming that tides were necessary for the formation of LSWL. Zhang et al. (2014a, b) analyzed the evolution of the vertical salinity structure in the detachment region from neap tide to spring tide and suggested clear vertical salinity stratification during the neap tide period; further, these authors indicated that the tide-induced vertical mixing gradually strengthened from neap tide to spring tide and that the surface salinity in the shallow water increased faster than that in the deep water, which was helpful for forming the LSWL. In Fig. 10, we examine the vertical salinity structure along Line B (marked in Fig. 5b) in CASE06. The variation in the salinity distribution from neap tide (August 3) to spring tide (August 10) was consistent with the numerical simulation results of Zhang et al. (2014a, b). The results demonstrate that tidal mixing may be attributed to detachment.

To examine the role of tidal mixing in the detachment discussed above, we tried to eliminate tidal mixing. In CASE06d, the coefficients of the vertical eddy diffusivity (K_h) are set to 0, while all other settings are consistent with those in CASE06. Compared with Fig. 5, the spatial pattern of CDW patches in CASE06d exhibits major alterations. The low-salinity water quickly extended farther northeastward and clearly detached from the interior side of the river plume at approximately 32.2°N, 122.2°E (Fig. 11a). These results reflect that tidal mixing played a limited role in detaching the LSWL.

4.3 *Upwelling and the detachment mechanism*

Figure 7 also shows the 5-day average vertical velocity in the 0–10 m layer from August 2 to 21, 2006 in CASE06. During August 2 to 6, the upwelling was distributed mainly along the coastline of Jiangsu and near the Changjiang River Estuary, and the maximum upwelling velocity was approximately 0.3×10^{-4} m/s. During August 7 to 11, upwelling occurred along the 30 m isobath at a mean speed of 0.10×10^{-4}–0.27×10^{-4} m/s. During August 12 to 16, the upwelling along the 30 m isobath was slightly weakened, and after August 16, nearby upwelling disappeared from the study area.

Figure 12 shows the effects of upwelling on the detachment along Line C during August 7 to 11 in CASE06. Significant upwelling occurred in the region with a water depth of approximately 30 m, and the maximum velocity was approximately 0.3×10^{-4} m/s. The 28 isohaline, which is located at a depth of 30 m, was uplifted by upwelling, which brought high-salinity water to

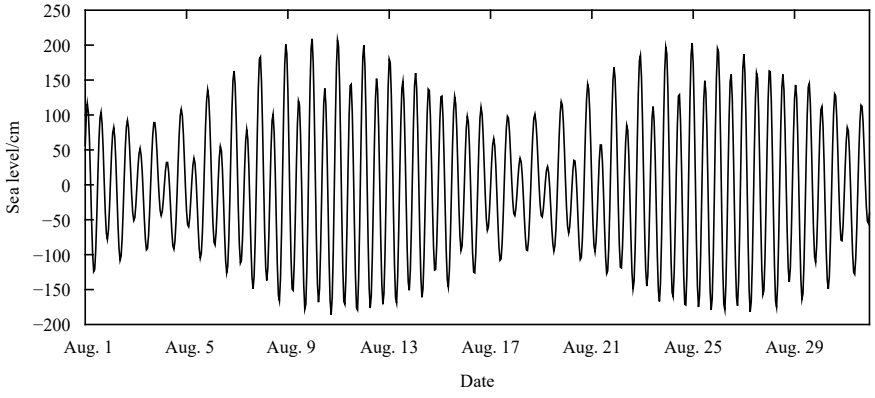

Fig. 9. Tide level at Lühuashan station from August 1 to 31 in 2006 (the reference level is the average sea level).

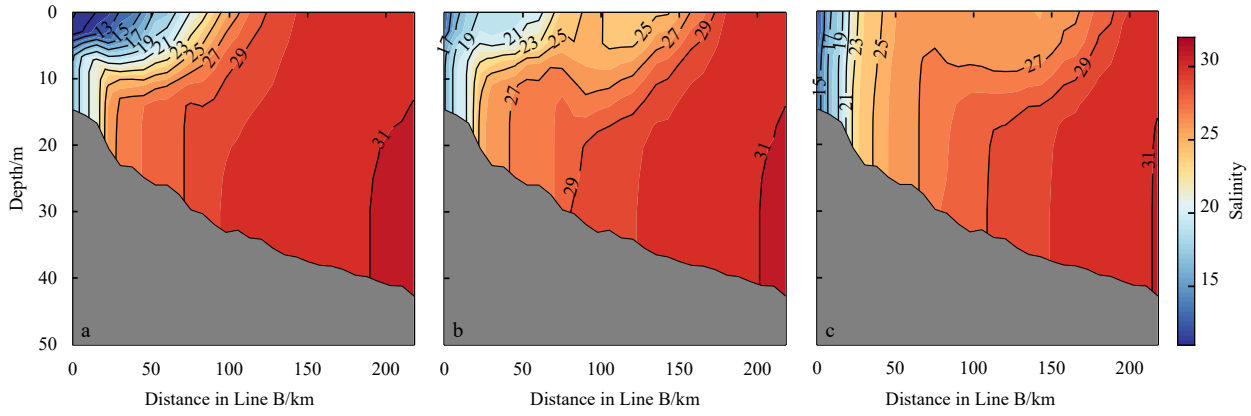

Fig. 10. Vertical distributions of salinity along Line B in CASE06 on August 3 (a), August 7 (b) and August 10 (c).

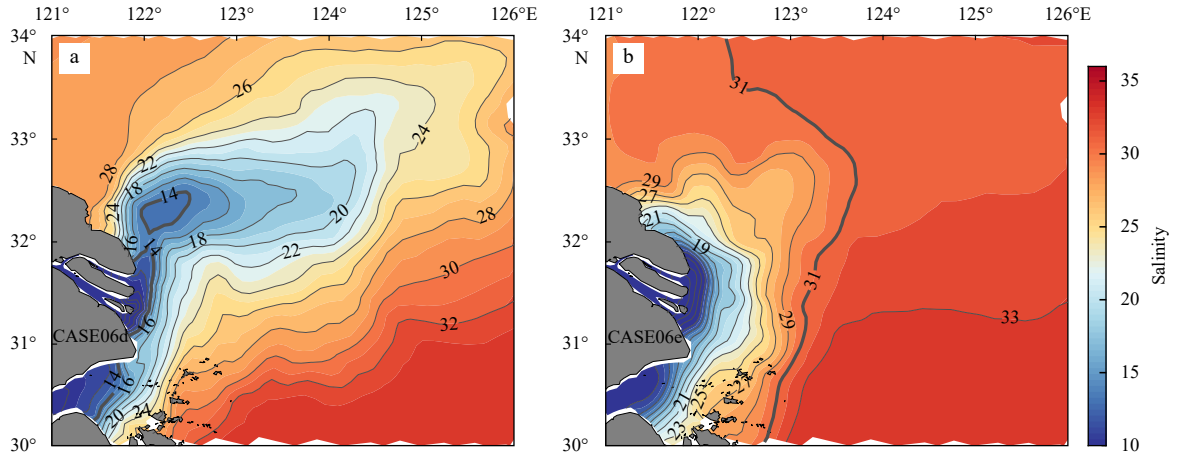

Fig. 11. Surface distributions of salinity in CASE06d at 18:00 on August 4 (a) and in CASE06e at 01:00 on August 12 (b).

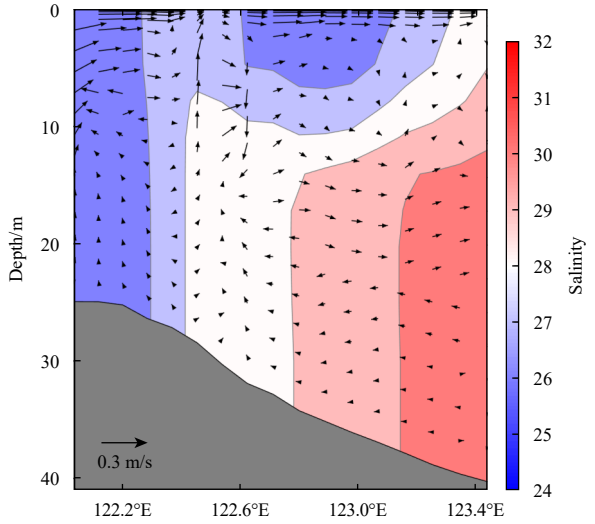

Fig. 12. Vertical salinity and upwelling distributions along Line C (marked in Fig. 5c) in CASE06. The upwelling is the average result from August 7 to 11. The upwelling velocity is amplified by a factor of 10^4. Salinity is the simulated result at 01:00 on August 12.

the surface layer and disconnected part of the Changjiang River plume. This upwelling event can be validated with previous observations. Hu and Zhao (2008) used remote sensing data to investigate upwelling events in the coastal area of Zhejiang and found that upwelling is generally located around the 30 m isobath, which is similar to the results of this paper.

The evolutionary characteristics of these upwelling phenomena and the LSWL were closely related. The strong upwelling along the coast brought high-salinity water from the deeper layer to the surface layer during August 2 to 6. This upwelling served to cut off the CDW vertically. Under the influence of strong upwelling in the detachment region, an isolated LSWL quickly appeared. During August 7 to 11, the LSWL moved northeastward, with a new upwelling area appearing along the 30 m isobath. The upwelling weakened slightly from August 12 to 16 but nevertheless cut off the CDW continuously, thereby stabilizing the LSWL.

If w_z and ω are the vertical velocities in the z and σ coordinates, respectively, the transform between w_z and ω is

$$w_z = D\omega + (1+\sigma)\frac{\partial \zeta}{\partial t} + u\left(\frac{\partial \zeta}{\partial x} + \sigma\frac{\partial D}{\partial x}\right) + v\left(\frac{\partial \zeta}{\partial y} + \sigma\frac{\partial D}{\partial y}\right). \quad (7)$$

The numerical simulation CASE06e was conducted to quantify the effects of upwelling on the detachment of the LSWL. In CASE06e, ω in Eq. (7) is replaced with the variable ω_s, resulting in $w_z = 0$:

$$\omega_s = -\frac{1+\sigma}{D}\frac{\partial \zeta}{\partial t} - \frac{u}{D}\left(\frac{\partial \zeta}{\partial x} + \sigma\frac{\partial D}{\partial x}\right) - \frac{v}{D}\left(\frac{\partial \zeta}{\partial y} + \sigma\frac{\partial D}{\partial y}\right). \quad (8)$$

When using Eq. (5) to calculate salinity, the particle location of point P at time $n\Delta t$ is traced back using the velocity (u, v, ω_s) from point Q at time $(n+1)\Delta t$. The other settings for CASE06e are the same as those for CASE06.

No detachments formed during the entire simulation of CASE06e. Figure 11b shows the simulated surface salinity at 01:00 on August 12 in CASE06e. Compared with the results depicted in Fig. 5c, the results of CASE06e deviate considerably. The expansion area shrank remarkably and the main body of the CDW was closer to the coast. The outer boundary of the CDW is always defined by a salinity of 31 (Gong et al., 1996; Zhao, 1993). The two simulations differed in the expansion range. The 31 isohaline in CASE06 extended eastward to 124.8°E, while this isohaline extended to only 123.8°E in CASE06e. Although the CDW in CASE06e still tended to expand northeastward, due to the lack of the vertical cutting force of upwelling, it was impossible to isolate the LSWL.

4.4 *Baroclinic effect and the detachment mechanism*

Two numerical simulations, CASE06f and CASE06g, were conducted to test the baroclinic effect on the LSWL. In CASE06f, the influence of the baroclinic effect was not considered at all; similarly, in CASE06g, the baroclinic feedback effect caused by changing salinity was not considered.

Figure 13a shows part of the simulated surface salinity for CASE06f. Beginning on August 1, the CDW expanded with a pattern resembling a narrow tongue toward the northeast. At 15:00 on August 12, the LSWL detached from the interior side of the river plume at approximately 32.6°N, 122.9°E and disappeared at 20:00 on August 13. The value of the outermost closed isohaline was 25, and the size of this LSWL was 65 km.

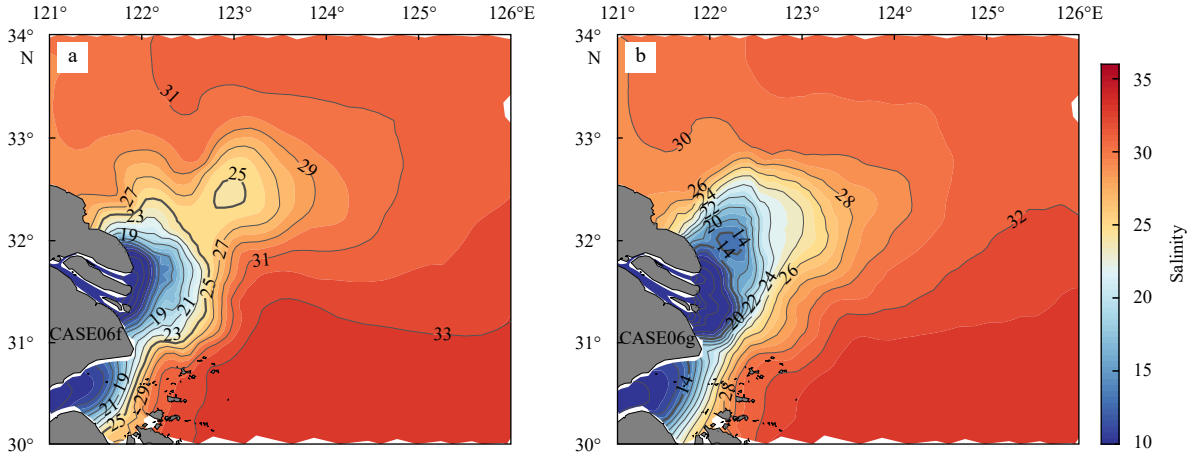

Fig. 13. Surface distribution of salinity in CASE06f at 01:00 on August 13 (a) and in CASE06g at 05:00 on August 6 (b).

Figure 13b shows part of the simulated surface salinity for CASE06g. Beginning on August 3, the CDW spread from south to north. At 05:00 on August 6, the LSWL detached from the interior side of the river plume at approximately 32°N, 122.2°E and then gradually moved northeastward. Finally, the LSWL disappeared at 06:00 on August 12. From August 6 to 12, the LSWL disappeared briefly several times, the CDW maintained a tongue pattern, and the value of the central closed isohaline of the LSWL increased from 14 to 25. The size of the LSWL was generally 27–40 km.

In comparison with that shown in Fig. 5a, the CDW of CASE06f expanded northeastward in a narrower tongue pattern. Additionally, the LSWL lasted for a shorter time than that in CASE06. The baroclinic feedback effect was not considered in CASE06g, and the expansion pattern of the CDW changed little, while the LSWL lasted for a slightly shorter time.

5 Upwelling mechanism analysis

According to previous studies, the formation mechanisms responsible for upwelling are diverse. Lü et al. (2006) suggested that tidal mixing plays a dominant role in inducing upwelling. Additionally, topography exerts profound influences on upwelling. Zhu (2003) studied the upwelling off the Changjiang River Estuary by conducting numerical tests and proposed that in the northern submarine valley the baroclinic effect primarily accounts for upwelling. Zhao et al. (2003) found that the upwelling off the Changjiang River Estuary was induced by the interaction between the TWC and the slope bottom topography and that the southerly wind had an important impact on the upwelling in the upper layer. Ni et al. (2014) suggested that the Coriolis force and pressure gradient force were the main forcing factors for the upwelling off the Changjiang River Estuary.

As previously discussed, four experiments (Table 2) were designed to examine the influences of the baroclinic effect, wind forcing, and tides on upwelling during the evolution of the LSWL. The CASE06h experiment was designed to analyze the influences of the baroclinic effect on the upwelling, and the same model settings for CASE06 were used for CASE06h except that the salinity of this experiment was fixed and the BPG was set to 0. To analyze the influences of the wind forcing and tides on upwelling and to avoid the indirect effects of salinity changes, the arrangements of CASE06i and CASE06j, which were based on CASE06h, eliminated the wind forcing and tide components, respectively. For CASE06k, the effects of all dynamic factors except tides were removed. These four experiments were used to simulate the currents during August 2 to 21.

Table 2. Summary of the numerical experiments conducted to analyze the upwelling mechanism[1)]

Case	Baroclinity	Wind	Tide	River discharge and open boundary current
CASE06h	N[2)]	Y	Y	Y
CASE06i	N[2)]	N	Y	Y
CASE06j	N[2)]	Y	N	Y
CASE06k	N[2)]	N	Y	N

Note: [1)] Y means that the dynamic factors were considered in the simulation, and N means that the dynamic factors were excluded from the simulation. [2)] The salinity of this experiment was fixed and the BPG was set to 0.

5.1 *Influences of the baroclinic effect on upwelling*

The simulation results showed that the upwelling distribution of CASE06h (Fig. 14) during August 7 to 11 was different from that of CASE06 (Fig. 7b), although these differences were not obvious in some areas. The intensity of upwelling in the sea north of 32°N slightly increased, and the upwelling patterns exhibited few alterations. The upwelling patterns south of 32°N showed more obvious changes than those in the north. Moreover, the upwelling area near the Changjiang River Estuary moved offshore with a slightly decreased intensity in CASE06h and a new upwelling area appeared near the Zhoushan Islands. The upwelling distributions in the other periods of August 2 to 21 did not change much compared with those in CASE06.

5.2 *Influences of the wind forcing on upwelling*

Wind-driven upwelling is a classic conceptual model for upwelling on inner shelves. In coastal seas, the steady blowing of winds that promote for upwelling drives the surface water to

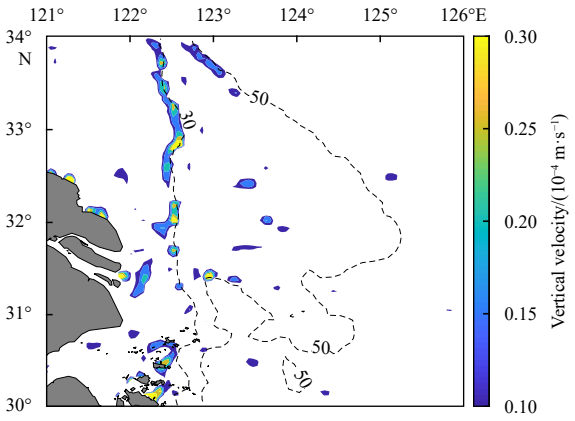

Fig. 14. Distribution of the 5-day average vertical velocity in the 0–10 m layer during August 7 to 11 in CASE06h. Dashed lines are the 30 m and 50 m isobaths.

move offshore within the surface Ekman layer. Divergence along the coast is created, and deeper water must move onshore and toward the surface to maintain mass conservation.

Compared with the results in Fig. 6a, CASE06i shows a large vertical change from August 2 to 6 (not shown). The upwelling area along the Jiangsu coast and near the Zhoushan Islands nearly disappeared. During August 7 to 21, the general upwelling patterns in the CASE06i exhibited few alterations: during August 7 to 16, there were two strong upwelling areas in the northeast sea off the Changjiang River Estuary and along the 30 m isobath in both CASE06h and CASE06i, while the upwelling was weak during August 17 to 21. The differences between CASE06h and CASE06i suggest that the upwelling along the Jiangsu coast during August 2 to 6 was induced by the persistent southeasterly wind. However, winds played a limited role in inducing upwelling during August 7 to 16.

5.3 *Influences of tides on upwelling*

Lü et al. (2007) used the Marine Science and Numerical Modeling (MASNUM) wave-tide-circulation coupled numerical model to simulate the upwelling patterns off the Changjiang Estuary and in the adjacent waters off the Zhejiang coast, and the results suggested that tidal mixing plays a dominant role in inducing upwelling. To analyze the tidal influences on upwelling and avoid the indirect effects of salinity changes on upwelling, CASE06j was designed based on CASE06h but with the elimination of tides.

Compared with those of CASE06h, the upwelling areas of CASE06j from August 2 to 6 exhibited few alterations. However, from August 7 to 16, the upwelling areas along the 30 m isobath disappeared (not shown). The differences between CASE06h and CASE06j indicate that the upwelling during August 7 to 16 was induced by tides.

Comparing the evolution of the upwelling (Fig. 7) with the tide level at Lühuashan station (Fig. 9), we find a significant upwelling response to the spring-neap tide modulation along the 30 m isobath. During the neap tide period (August 2 to 6), the upwelling along the 30 m isobath was weak. Subsequently, as the spring tide arrived (August 7 to 11), the tidal forcing was gradually strengthened, which induced strong upwelling along the 30 m isobath. As the tidal forcing weakened during the transition time from spring tide to neap tide (August 12 to 16), the upwelling became weaker than that in the last phase. Finally, upwelling disappeared during the neap tide period (August 17 to 21).

To further verify the effects of tides on the upwelling, the upwelling on August 3, 7, and 10 was simulated by CASE06i according to the tide level at Lühuashan station. The simulated results are shown in Fig. 15. For the study region, only very weak upwelling was present at neap tide (August 3). The upwelling along the 30 m isobath gradually appeared; finally, the vertical velocity reached its maximum at spring tide (August 10). These simulation results confirm that the upwelling along the 30 m isobath was induced predominantly by tides.

To determine the dynamics of the upwelling under the interactions of tides and topography, CASE06k was employed to simulate the ERC at spring tide (August 10). Figure 16 shows the distribution of the bottom ERC ($\sigma = -0.93$). The ERC near the coastal area with depths shallower than 30 m flowed offshore at a speed of 3–5 cm/s; in the sea area north of 32°N, the bottom ERC flowed onshore across the 30 m isobath at a speed of 1–2 cm/s. On one hand, the tidal residual currents converged at the 30 m isobath and induced an upwelling band. On the other hand, the inclined slope helped the tidal residual current upwell because the bottom topography provided an inclined plane up which the bottom currents could climb (Lü et al., 2006).

6 Discussion and conclusions

By combining observed temperature and salinity data, we found an isolated LSWL offshore from the Changjiang River Estuary in August 2006. The LSWL isolated by the 22 isohaline had an elliptical shape, and the value of the center closed isohaline was 20 psu. The vertical structures of the salinity and temperature along Line A indicated that cold and saline deep water upwells along the bottom slope.

In this study, the POM-σ-z model was used to simulate the LSWL in the summer of 2006 and the simulated results indicate that the LSWL became detached at the interior side of the river plume and persisted during August 7 to 19. At the beginning of the detachment, the LSWL had a low salinity, although as the LSWL moved offshore, the central salinity value increased due to mixing with high-salinity water.

Winds played important roles in the formation and evolution of the LSWL. During August 2 to 6, the persistent southeasterly wind induced the northwestward expansion of the LSWL. ERC vectors, which imposed an uneven northward force on the CDW, showed differences between the nearshore and far-shore detachment regions. Strong upwelling occurred along the Jiangsu coast and off the Changjiang River Estuary, and it carried high-salinity water to the surface layer and strengthened vertical mixing, which was favorable for the detachment of the LSWL. During August 7 to 11, with the continued easterly wind, the northeastward ERC in the detachment region was conducive to driving the LSWL offshore. A new upwelling area appeared along the 30 m isobath, which stabilized the LSWL. During August 12 to 16, the light wind in the study region weakened the ERC and the upwelling; hence, the LSWL remained steady. After August 17, the upwelling disappeared and the strong southwestward ERC induced by the strong northerly wind drove the LSWL onshore, which caused the LSWL area to decrease gradually until it disappeared.

Numerical experiments showed that tides are a necessary condition for the formation of LSWLs. Zhang et al. (2014a, b) indicated that tide-induced vertical mixing gradually strengthens from neap tide to spring tide, which is helpful for forming a LSWL. However, an interesting phenomenon presented herein is that the LSWL did not disappear when vertical mixing ceased. These results indicated that the tide affects detachment by phys-

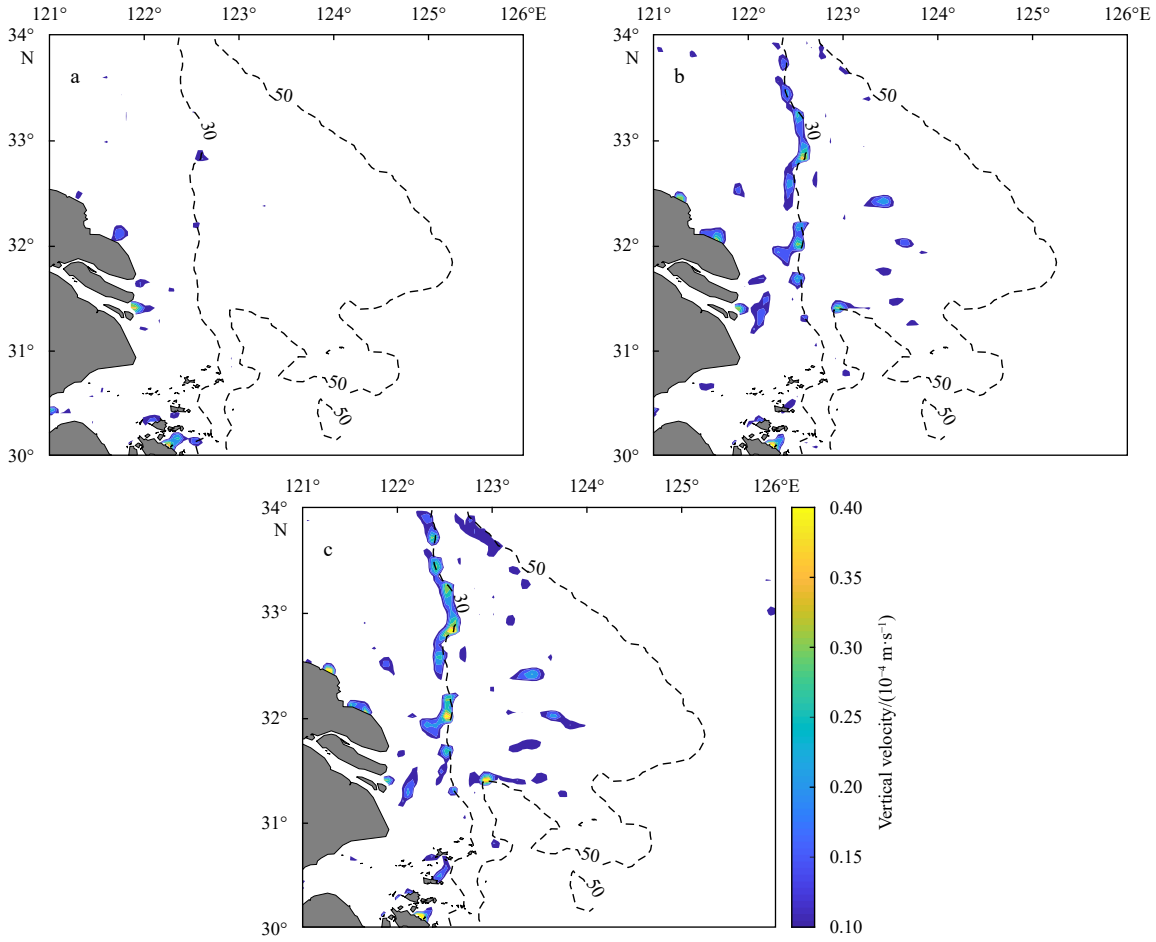

Fig. 15. Distribution of vertical velocity in the 0–10 m layer on August 3, 7, and 10 simulated by CASE06i. Dashed lines are the 30 m and 50 m isobaths.

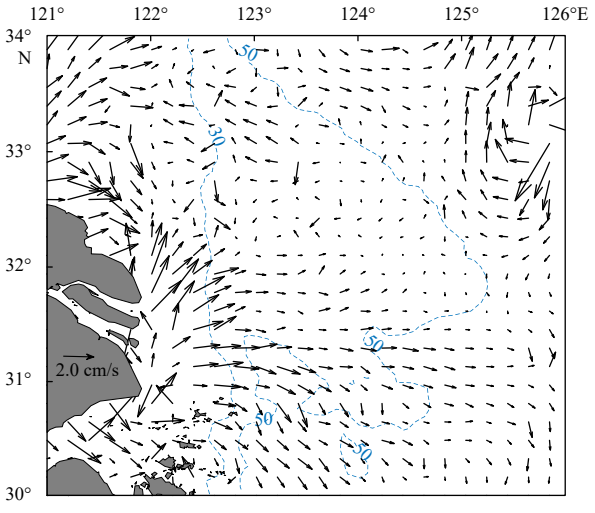

Fig. 16. Distribution of bottom currents (vectors, σ=–0.93) on August 10 simulated by CASE06k. Blue dashed lines are the 30 m and 50 m isobaths.

ical processes other than tidal mixing.

Upwelling is crucial in detachment events. Furthermore, the influences of three dynamic mechanisms on upwelling, namely, the baroclinic effect, wind forcing and tides, were also discussed. The baroclinic effect played only a limited role in the upwelling along the Jiangsu coast and in the northeast sea off the Changjiang River Estuary. The persistent southeasterly wind during August 2 to 6 induced strong upwelling near the Changjiang River Estuary and along the Jiangsu coast; however, the direction and intensity of the wind during August 7 to 21 were not conducive to inducing upwelling. Tide-induced upwelling gradually increased during the transition from neap tide to spring tide. The bottom ERC near the coastal area with depths shallower than 30 m flowed offshore, and in the sea area north of 32°N, the bottom ERC flowed onshore across the 30 m isobath at spring tide. The tidal residual currents converged at the 30 m isobath, and the bottom topography provided an inclined plane that the bottom ERC could climb.

The distribution of nutrients and dissolved oxygen is greatly affected by LSWLs. In particular, detachment will change the local ecological environment. Our work can therefore provide theoretical suggestions for the protection of ecological environments and aquaculture in the Changjiang River Estuary. However, there are still many unclear aspects; for example, the TWC and Changjiang River discharge may affect the upwelling near the Changjiang River mouth. Therefore, more numerical simulations are needed for further study.

References

Blumberg A F, Mellor G L. 1987. A description of a three-dimensional

coastal ocean circulation model. In: Heaps N S, ed. Three-dimensional Coastal Ocean Models. Washington: American Geophysical Union, 1–16

Chen Changsheng, Xue Pengfei, Ding Pingxing, et al. 2008. Physical mechanisms for the offshore detachment of the Changjiang diluted water in the East China Sea. Journal of Geophysical Research, 113(C2): C02002

Hu Mingna, Zhao Chaofang. 2008. Upwelling in Zhejiang coastal areas during summer detected by satellite observations. Journal of Remote Sensing (in Chinese), 12(2): 297–304

Kim H C, Yamaguchi H, Yoo S, et al. 2009. Distribution of Changjiang diluted water detected by satellite chlorophyll-*a* and its interannual variation during 1998–2007. Journal of Oceanography, 65(1): 129–135, doi: 10.1007/s10872-009-0013-0

Li Li, Cen Jingyi, Cui Lei, et al. 2019. Response of size-fractionated phytoplankton to environmental factors near the Changjiang Estuary. Acta Oceanologica Sinica, 38(1): 151–159, doi: 10.1007/s13131-018-1259-4

Li Mingming, Xie Lingling, Zong Xiaolong, et al. 2018. The cruise observation of turbulent mixing in the upwelling region east of Hainan Island in the summer of 2012. Acta Oceanologica Sinica, 37(9): 1–12, doi: 10.1007/s13131-018-1260-y

Li Daoji, Zhang Jing, Huang Daji, et al. 2002. Oxygen depletion off the Changjiang (Yangtze River) Estuary. Science in China Series D: Earth Sciences, 45(12): 1137–1146, doi: 10.1360/02yd9110

Lie H J, Cho C H, Lee J H, et al. 2003. Structure and eastward extension of the Changjiang River plume in the East China Sea. Journal of Geophysical Research, 108(C3): 3077, doi: 10.1029/2001JC001194

Lü Xingang, Qiao Fangli, Xia Changshui, et al. 2006. Upwelling off Yangtze River estuary in summer. Journal of Geophysical Research, 111(C11): C11S08

Lü Xingang, Qiao Fangli, Xia Changshui, et al. 2007. Tidally induced upwelling off Yangtze River estuary and in Zhejiang coastal waters in summer. Science in China Series D: Earth Sciences, 50(3): 462, doi: 10.1007/s11430-007-2050-0

Moon J H, Hirose N, Yoon J H, et al. 2010. Offshore detachment process of the low-salinity water around Changjiang bank in the east China sea. Journal of Physical Oceanography, 40(5): 1035–1053, doi: 10.1175/2010JPO4167.1

Ni Tingting, Guan Weibing, Cao Zhenyi, et al. 2014. Numerical study on the upwelling of Zhejiang coast in spring. Journal of Marine Sciences (in Chinese), 32(2): 1–13

Peng Jian, Zhu Shouxian, Li Xunqiang, et al. 2014. Impact of wind on the low-salinity water lens in the northeast out of the Changjiang Estuary in summer. Journal of East China Normal University (Natural Science) (in Chinese), (3): 105–116

Pu Yongxiu. 2002. The summer salinity distribution types of the 30°N profile in the East China Sea. Donghai Marine Science (in Chinese), 20(1): 1–13

Wang Kaimin, Xiong Xuejun, Guo Binghuo, et al. 2012. The extension form and seasonal variation of the Changjiang diluted water during 2006–2007. Coastal Engineering (in Chinese), 31(1): 46–54

Wu Qiong, Wang Xiaochun, Liang Wenhao, et al. 2020. Validation and application of soil moisture active passive sea surface salinity observation over the Changjiang River Estuary. Acta Oceanologica Sinica, 39(4): 1–8, doi: 10.1007/s13131-020-1542-z

Wu Hui, Zhu Jianrong, Shen Jian, et al. 2011. Tidal modulation on the Changjiang River plume in summer. Journal of Geophysical Research, 116(C8): C08017

Xuan Jiliang, Huang Daji, Zhou Feng, et al. 2012. The role of wind on the detachment of low salinity water in the Changjiang Estuary in summer. Journal of Geophysical Research, 117(C10): C10004

Zhang Tingting, Zhao Feng, Wang Sikai, et al. 2019. Estimating the macrobenthic species richness with an optimized sampling design in the intertidal zone of Changjiang Estuary. Acta Oceanologica Sinica, 38(2): 114–124, doi: 10.1007/s13131-019-1352-3

Zhang Wenjing, Zhu Shouxian, Dong Lixian, et al. 2011. A new hybrid vertical coordinate ocean model and its application in the simulation of the Changjiang diluted water. China Ocean Engineering, 25(2): 327–338, doi: 10.1007/s13344-011-0027-4

Zhang Wenjing, Zhu Shouxian, Li Xunqiang, et al. 2014a. Numerical simulation and dynamical analysis for low salinity water lens in the expansion area of the Changjiang diluted water. China Ocean Engineering, 28(6): 777–790, doi: 10.1007/s13344-014-0060-1

Zhang Wenjing, Zhu Shouxian, Li Xunqiang, et al. 2014b. Impact of tide induced residual current and tidal mixing on the low salinity water lens in the northeast out of the Changjiang Estuary. Haiyang Xuebao (in Chinese), 36(3): 9–18

Zhao Baoren. 1993. The upwelling off Yangtze River Estuary. Haiyang Xuebao (in Chinese), 15(2): 108–114

Zhao Baoren, Li Huifei, Yang Yuling. 2003. Numerical simulation of upwelling in the Changjiang River mouth area. Studia Marina Sinica (in Chinese), (45): 64–76

Zhu Jianrong. 2003. Dynamic mechanism of the upwelling on the west side of the submerged river valley off the Changjiang mouth in summertime. Chinese Science Bulletin, 48(24): 2754–2758, doi: 10.1007/BF02901770

Zhu Shouxian, Ding Pingxing, Sha Wenyu, et al. 2001. New Eulerian-Lagrangian method for salinity calculation. China Ocean Engineering, 15(4): 553–564